3

Polymer Holography in Acrylamide-Based Recording Material

Milan Květoň[1], Pavel Fiala[2] and Antonín Havránek[3]
[1,2]*Czech Technical University in Prague, Faculty of Nuclear Sciences and Physical Engineering, Department of Physical Electronics*
[3]*Charles University, Faculty of Mathematics and Physics, Department of Macromolecular Physics*
Czech Republic

1. Introduction

Photopolymers are attractive recording materials for different holographic applications such as image holography, holographic memories, diffractive optical elements, or holographic interferometry (Hariharan (1996)). They differ from traditionally used silver-halide emulsions or dichromated gelatin (Bjelkhagen (1996)) in their self-developing characteristics. A hologram in a photopolymer is formed already during exposure of the interference field and no additional wet developing process is needed. The first photopolymer recording media were prepared by Close et al. (1969). Since then, numerous systems have been examined but only a small number become suitable for holographic applications. Companies such as DuPont, InPhase, or Polygrama produce commercial photopolymer systems. However, the exact chemical composition is not known and is proprietary. This fact complicates both experimental and theoretical studies of recording processes which is necessary for understanding of behavior of the recording material. Next to the commercial systems, photopolymers can be also prepared in a laboratory. Its chemical composition is known and can be modified, if we need to study the response on material components. This makes the laboratory prepared photopolymers interesting for the research even if their sensitivity, resolution, refractive index change, or stability are often lower in comparison with commercial systems.

In our holographic laboratory, we prepare, test, and apply different types of recording media. If we use traditional recording materials, we often get on their limits. For example, a thick layer of silver-halide emulsion is difficult to fabricate and process. But only gratings formed in thick layers have high angular selectivity and diffraction efficiency which is required for high capacity holographic recording media. Photopolymers can be prepared in thicknesses ranging from 10-1000 μm. They are also much more convenient for holographic interferometry due to their self-developing ability. However, recording mechanisms running during holographic exposure are still not fully understood and so they can not be effectively used. For our experimental study on photopolymers, the acrylamide-based material was chosen for the following reasons. It is composed of available chemicals, it can be prepared in our laboratory and its composition can be easily modified to produce samples for different tests. The used photopolymer system with acrylamide monomer, triethanol amine initiator,

and polyvinyl alcohol binder was described in the late 1980s by Calixto (1987). Martin et al. (1994) optimized the composition for recording in the green region of the visible spectrum by the addition of a xanthene dye. Acrylic acid as the second co-monomer was introduced into the recording system by Xia et al. (2002). The characteristics of the acrylamide-based photopolymer have been already studied by several authors: Babeva et al. (2008); Martin et al. (1997); Naydenova et al. (2004); Neipp et al. (2003), etc. Within our research on the acrylamide-based recording material, we have modified its chemical composition to obtain more sensitive recording material with higher final value of the refractive index modulation in comparison with other acrylamide-based photopolymers. We have also extended the standard real-time measurement method. Next to the real-time measurement of a growth of the first harmonic grating, we have simultaneously measured a growth of the second harmonic grating that gives a better idea about the non-linear recording process. Some of the results have been already published (Květoň et al. (2007; 2008)).

Next to the experimental works, theoretical models of polymer recording have been developed. Zhao & Mouroulis (1994) proposed one dimensional diffusion model. The model assumes that a growing polymer chain is located at its place of origin. The diffusion equation, which describes polymerization and diffusion processes of monomers, was solved and the model predicts failure of the reciprocity law for intensity and time and the low spatial frequency cut-off. Colvin et al. (1997); Kwon et al. (1999) revised the model and specified more exactly process of the linear radical chain polymerization. With the basic diffusion model, the high spatial frequency cut-off is not possible to explain. Therefore, a non-local response function was introduced to the diffusion equation by Sheridan & Lawrence (2000). The extended model assumes that a polymer chain grows away from its place of initiation and so its size limits the resolution of the recording medium. The non-local polymerization driven diffusion model has been continuously improved, additional processes running during the holographic exposure have been included. A detail review of the non-local modelling was elaborated by Gleeson & Sheridan (2009). Our contribution to the topic of polymer recording is the immobilization-diffusion theory (ID-theory). The theory is based on the fact that also a growing polymer can move and its mobility successively decreases with its polymerization degree (Havránek & Květoň (2008); Havránek et al. (2007)).

Having in mind the goal of the paper, i.e. to explain the process of polymer recording and present our experimental findings obtained with acrylamide-based photopolymer, the paper is organized as follows. The theory of polymer recording is introduced in section 2. The recording process is explained with the ID-theory and the basic simulations are presented. In section 3, the chemical composition of the acrylamide-based photopolymer and its preparation procedure is described. The principles of the characterization method, our setup, and processing of measured data are given in section 4. In the following section 5, our main experimental findings are presented. The material response depends on both exposure conditions and chemical compositions. Hence, an influence of different parameters is shown and discussed. Also the measurements of non-linearities, which form during the recording process, are studied. Finally, the paper is concluded.

2. Theory of polymer recording

The process of a diffraction grating record is complex and involves several mechanisms such as absorption of light, polymerization, and diffusion. Monomer and initiator are the most important components of the photopolymer recording material. The material is sensitive to a particular wavelength of light. If the material is exposed with the interference field,

absorption of light occurs and the polymerization reaction of monomer molecules is initiated. The polymerization rate alternates according to the intensity of illumination and so does the concentration of monomers. In intensity maxima, the amount of polymers rapidly increases and additional monomers flow from surroundings to homogenize the monomer concentration gradient. The mobility of a long polymer chain is very low in comparison with a monomer. Therefore polymers remain at their place of origin where their concentration increases and hence does the refractive index. The recording process is irreversible and a permanent refractive index grating is formed. In Fig. 1, the recording process is illustrated.

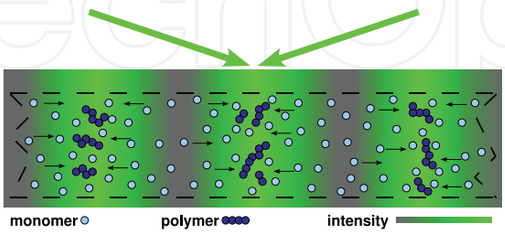

Fig. 1. Record of the harmonic interference field in a photopolymer material.

The briefly described recording process will be further formulated with our ID-theory and some basic simulations of the theoretical model will be presented.

2.1 Immobilization-diffusion theory

The main idea of the new theory, which we denoted immobilization-diffusion theory, is the fact that the mobility of polymer chains decreases as they grow. The mobility of dimers, trimers and other short oligomers is comparable with that of monomers whereas the mobility of polymer chains with higher polymerization degree (number of monomer units of which the polymer is composed) is negligible. The standard diffusion theories neglect the mobility of short oligomers and suppose that the position of a polymer is fixed from the very beginning of its growth. The typical S-shape form of the measured refractive index modulation grow-curves is in contradiction with this simplified assumption. The ID-theory has been created to explain the S-shape of the measured grow-curves. The ideas of the ID-theory will be described at first for one isolated polymer chain and then it will be extended to the real situation when polymers start to grow with some space and time distribution.

2.1.1 Single polymer case

Schematic view of the recording medium with the coordinate system used in further calculations is given in Fig. 2. The number of monomers in a unit volume of the medium is denoted as the monomer concentration $C_m = C_m(x, y, z)$. Only the x-direction dependence $C_m = C_m(x)$ is supposed in the forthcoming calculations. Neglecting the finite dimensions of the exposed film in z-direction leading to ignoring the z-dependence of C_m is not a crude approximation. But the dependence of C_m on the y-coordinate may be important as the thickness of the film ($>10\,\mu$m) is substantially larger than monomer dimensions and the illumination profile may be changed substantially along the y-coordinate. In more refine calculations, the dependence of C_m on y probably cannot be neglected.

Now, we shall study how moves the polymer that starts to grow at the plane $x = 0$. The probabilities to move in $+x$ and $-x$ directions are the same and so, as the mobility of a polymer decreases with increasing polymerization degree k, the polymer moves closer and closer to the plain $x = 0$ at which it starts to grow. The start of the polymerization process

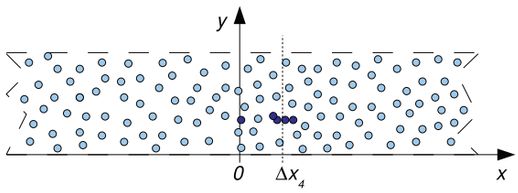

Fig. 2. A schematic view of the recording medium with one quadrimer which actual distance from the plane $x = 0$, where the polymer started to grow, is Δx_4.

means that two monomers join and then other monomers join the developing polymer chain. Polymer chain with low number of monomers is called oligomeric chain or oligomer. Mobility of the oligomer decreases with increasing number of joined monomers and it concentrates near the plain $x = 0$. So the homogeneity of the monomer concentration C_m in the film is disrupted and the modulation of it occurs.

The polymer grows as the monomer units join it. In the intervals Δt_k, monomers are added to the growing polymer chain, k is the polymerization degree. The polymer loses its mobility with increasing k; its probable deviation (actual value of this deviation for quadrimer $k = 4$ is denoted Δx_4 in Fig. 2) from the initial position ($x = 0$) decreases. We assume that

$$\Delta x_k = \frac{\Delta x_1}{k^m}, \ \mathrm{k} = 1, 2, 3 \cdots \tag{1}$$

Exponent m describes the rate of decrease and so the polymer immobilization. The exponent m has values between 0.5 and 1 if viscous random motion of a linear polymer is supposed. Higher values of m are obtained if some branching or cross-linking occurs. The probable deviation $\Delta x_1 = \Delta l_0/3$ where Δl_0 is the mean distance which a monomer molecule must undergo to reach another molecule at the beginning of the polymerization process. The factor $1/3$ is due to the fact that deviations only in the x-direction are concerned. During the polymerization process, the mean distance

$$\Delta l_k = \frac{1}{\sqrt{2} S C_{m,k}} \tag{2}$$

increases as the monomer concentration after k steps $C_{m,k}$ decreases as monomers are consumed by the polymer. The equation (2) is set in analogy to the derivation of the mean free path of molecules in the kinetic theory of gasses (see e.g. Reif (1965)). S is the effective cross-section of the radical through which the polymerization proceeds. The mean distance Δl increases as monomers are consumed by the polymer.

The next important point of the theory is that the deviation Δx_k is identified with the probable deviation δ_k of the Gaussian distribution function (e.g. Reif (1965));

$$|\Delta x_k| = \delta_k \doteq \frac{2}{3}\sigma. \tag{3}$$

Thus the probability $p_k(x)$ to meet the polymer of polymerization degree k at the distance $|x|$ from the plane $x = 0$ can be expressed as

$$p_k(x) = \frac{1}{\sqrt{2\pi}\sigma} \exp\left(-\frac{x^2}{2\sigma^2}\right) = \frac{2k^m}{\sqrt{2\pi}\Delta l_0} \exp\left(-\frac{2k^{2m}x^2}{\Delta l_0^2}\right), \tag{4}$$

where the mean free path of a monomer molecule Δl_0 was introduced in the second equation. The density $C_{p,k}$ of monomers incorporated in the growing polymer is obtained if the probability p_k is multiplied with the polymerization degree k;

$$C_{p,k}(x) = kp_k(x) = \frac{\sqrt{2}k^{m+1}}{\sqrt{\pi}\Delta l_0} \exp\left(-\frac{2k^{2m}x^2}{\Delta l_0^2}\right). \tag{5}$$

The drift of the polymer density towards the plane $x = 0$ with an increasing polymerization degree k is demonstrated in Fig. 3 for three values of k and three values of the exponent m. The stabilization of polymers in the vicinity of $x = 0$, where they have started to grow, is evident. The rate of stabilization increases with increasing m.

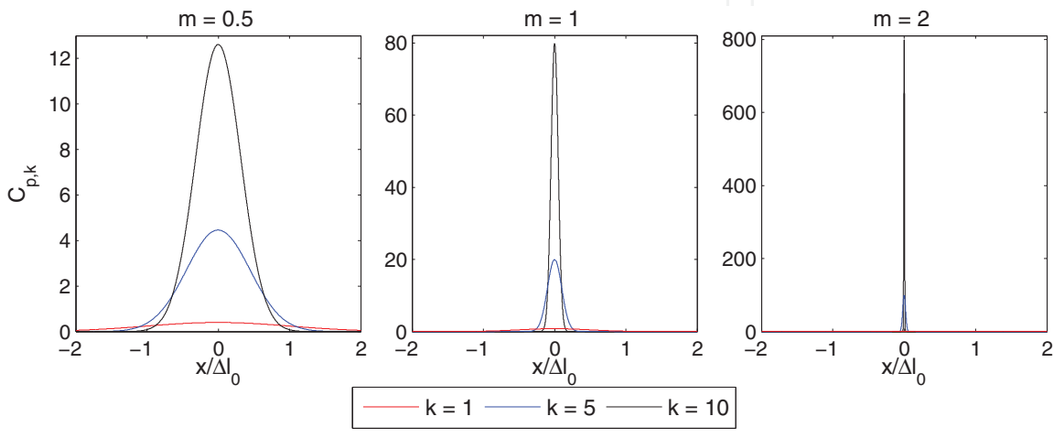

Fig. 3. Stabilization of the polymer near its initial position for three values of immobilization exponent m.

Now we shall study the time dependence of the process. As the free path Δl_k increases with increasing step k (see Eq. (2)) also the time interval Δt_k between two subsequent addings of monomers increases. If the time interval at initial concentration of free monomers C_{m0} is Δt_0, the interval after k steps is

$$\Delta t_k = \Delta t_0 \frac{P_0}{P_0 - k} \tag{6}$$

where P_0 is the total number of monomers in the area from which monomers arrive to our selected single polymer. The total time from the start of polymerization to the k step of it is the sum of the intervals given by Eq. (6);

$$t_k = \Delta t_0 \sum_{j=1}^{k} \frac{P_0}{P_0 - j}. \tag{7}$$

If we plot the density of polymers for $x = 0$, i.e. $C_{p,k}(0)$, against t_k we obtain the typical S-shaped grow-curve. Such a curve is given in Fig. 4 for $P_0 = 100$ and $m = 1$. The dots in the graph represent the individual k steps. The t_k axis is given in units Δt_0. The intervals between dots are the Δt_k values and they increase with increasing k in accordance with Eq. (6).
In this simplified model, the S-shape of the grow-curve may be well explained. At the beginning of the polymerization process (small k values), the immobilization of oligomers prevails and the slope of the grow-curve rises. At the end of the process, nearly all

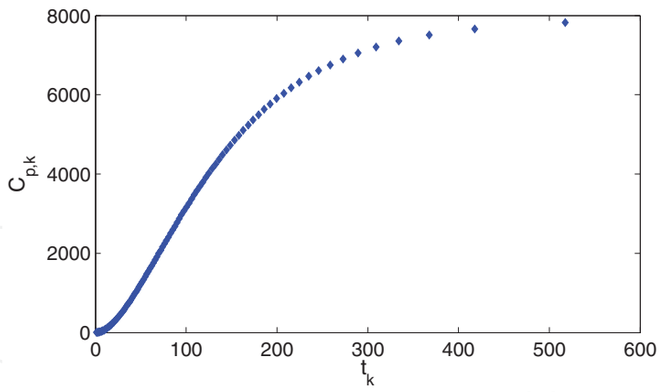

Fig. 4. The dependence of the density $C_{p,k}$ on time t_k for $m = 1$. Time and density are given in arbitrary units.

the monomers are consumed, the Δt_k intervals dramatically grow and the slope of the curve approaches zero value. Somewhere between, the two processes compensate and the grow-curve has its inflexion point.

2.1.2 Continuous spatial and time distribution of the growing polymers

The number of polymers, which start growing in the place of coordinate $x = u$ at time $t = T$, is introduced by the initiation rate $\mathcal{R}_i$. It is assumed that $\mathcal{R}_i$ can be expressed as

$$\mathcal{R}_i(u, T) = AI(u)C_m(T), \tag{8}$$

where A is a constant characterizing the efficiency of initiation, $I(u)$ defines the intensity of illumination and $C_m(T)$ is the concentration of monomer units at time T. We use this relation to include the effect that monomers are exhausted at later times of the exposure. The concentration of free monomers decreases according to the exponential law which can be expressed as

$$C_m(T) = C_{m0} \exp(-T/\tau), \tag{9}$$

where τ is the relaxation time, $C_m(T)$ is the actual and C_{m0} the initial density of free monomers. It is assumed that the concentration of monomers decreases homogeneously (concentration gradient does not arise) due to a high mobility of monomers and short diffusion distances in the recording medium. Next, we introduce the actual degree of conversion

$$d = \frac{C_{m0} - C_m(T)}{C_{m0}}. \tag{10}$$

The degree of conversion d is the ratio of monomers remaining free at time T to the initial number of monomers. The degree of conversion d corresponds in the continuous case to the polymerization step k of the single polymer case. Only the reduction to the number P_0 from Eq. (6) in the single polymer case must be done. Then we obtain for the time dependences of d and reduced k the expressions

$$k' = \frac{k}{P_0} = d(T) = 1 - \exp(-T/\tau). \tag{11}$$

The spatial and time density of monomers incorporated in growing polymers $C_p(x,t)$ may now be expressed as

$$C_p(x,t) = \int_0^t \int_{-\infty}^{\infty} k'(T)\mathcal{R}_i(T,u)p\left(k'(T), x-u\right) \mathrm{d}u\mathrm{d}T. \tag{12}$$

The relaxation time τ and distribution of the harmonic interference field $I(u)$ are given with the expressions

$$\tau = \frac{1}{m\rho\sqrt{I_0}} \quad \text{and} \quad I(u) = I_0\left(1 + V\cos\left(\frac{2\pi}{\Lambda}u\right)\right). \tag{13}$$

m is the immobilization coefficient, ρ is a coefficient that associates initiation, polymerization, and termination rate constants, I_0 is the overall intensity, V is the visibility or contrast of the inference fringes and Λ is the period of the interference field. If we introduce the relaxation time τ and the intensity distribution $I(u)$ in Eq. (12) and assume that the polymer density $C_p(x,t)$ is proportional to the distribution of the refractive index, we obtain after evaluation of the first harmonic amplitude the refractive index modulation

$$n_1(t) \propto \exp\left(-2m\sqrt{I_0}t\right)\left(1 - \exp\left(m\sqrt{I_0}t\right)\right)^2. \tag{14}$$

The proportionality constant depends especially on the initial concentration of monomers, the visibility and the intensity of light. For more details see (Havránek et al. (2007; 2008)).

2.1.3 Results of model calculations

The time dependence of the refractive index modulation $n_1(t)$, which describes the grating formation process, is named the grow-curve. The teoretical forms of the grow curves predicted by Eq. (14) are given in Fig. 5. The refractive index modulation at first rises with an increasing grow rate, goes through an inflexion point and with a decreasing grow rate, it achieves its maximum value at which all the monomers are consumed by polymers. The rate of this process depends on the immobilization parameter m and also on the intensity of illumination I_0 and visibility V.

The dependence of grow-curves on exponent m is illustrated in Fig. 5 (a) where the calculated reduced curves for three different values of the immobilization parameter m are given. It can be seen, that with increasing m, the curves become more abrupt and their points of inflexion occur at lower reduced time values. The grow-curves corresponding to higher values of m indicate that some faster mechanism of polymer growth, such as branching or network formation, probably occurs. The ID-theory prediction of the intensity dependence of grow-curves is given in Fig. 5 (b). Four curves, which mutual relative intensity differs ten times, are illustrated. The rate of growth increases with an increasing intensity of illumination and an earlier saturation occurs. Presented curves are normalized for a better comparison of the form of grow-curves with different exposure intensities. These curves correspond also with the results which were obtained with simulations of the diffusion model at different recording intensities.

The ID-theory coming out from very natural assumptions is able to explain the experimentally observed S-type form of the grow-curves. The predicted intensity dependence of theoretically obtained curves fits well with main features of experimentally observed curves. Branching or cross-linking during the polymerization process is introduced through the immobilization exponent m. The presented form of the theory is an elementary version with many approximations and simplifications. A dependence of the refractive index modulation on the

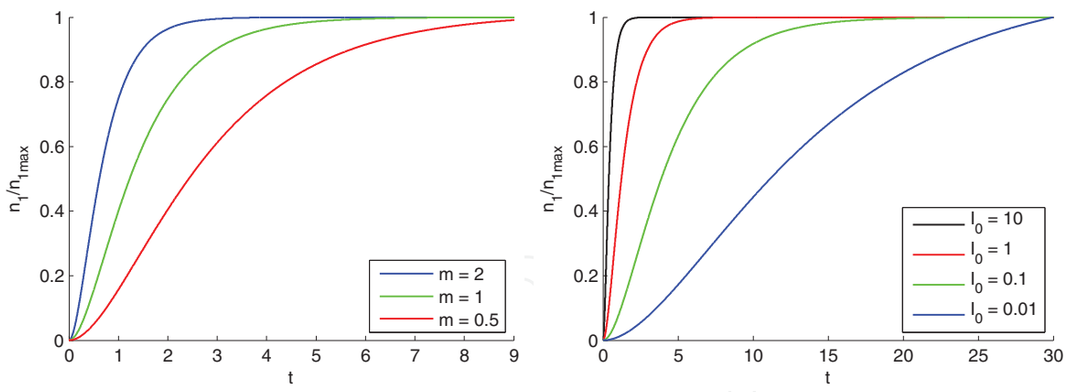

(a) different exponent m (b) different intensity I_0

Fig. 5. The normalized grow-curves for different values of the immobilization exponent m and recording intensity I_0. Time and intensity are given in relative units.

spatial period Λ and a formation of higher harmonics are not considered. A refinement of the theory will be possible after thorough analyzes of experimental results. Preliminary results will be shown and discussed further.

3. Recording material

For the measurements, the laboratory prepared acrylamide based photopolymer recording material is used. It is composed of acrylic monomers, polyvinyl alcohol binder, initiator and sensitizing dye. The prepared dry layers are typically 80 μm thick and are deposited on glass plates. The absorption maximum of the material is at a 537 nm wavelength (green light), its optimal exposure dose ranges from 20 to 40 mJ/cm^2, and the diffraction efficiency of a formed grating (volume phase transmission grating) reaches almost 100 %.

The chemical composition is based on the formula introduced by Martin et al. (1994). Within our experimental studies, concentrations of components and thickness of the material have been varied to obtain the optimal response for our experimental applications. All used chemicals are commercially available and they have been used without previous purification. The material is composed of the binder – polyvinyl alcohol (PVA), solid monomer – acrylamide (AA), liquid monomer – acrylic acid (AAC), crosslinker – N,N'-methylene-bis-acrylamide (BAA), initiator – triethanolamine (TEA), and sensitizing dye – erythrosine B (EB).

The chemical composition of the recording material, which is typically used for the measurements, is described in Tab. 1. The Solution I is prepared at first. PVA is dissolved in demineralized water and then 17 % water solution of PVA is produced. A normal white light room illumination can be used as PVA is not sensitive to a visible light. Then the Solution II is prepared. Components from the list (except Solution I) are put together and mixed well at first. It takes some time to dissolve the crosslinker. To this mixture, the appropriate amount of Solution I is added and mixed again. The viscous solution contains many air bubbles which might degrade the optical quality of the layer. Hence the solution is evacuated to release all unwanted bubbles. Red safe light must be used during the preparation procedure of the Solution II to avoid initiation of the polymerization reaction and thus a damage of the material.

The prepared solution is poured over a levelled glass plate, spread with a stick or other coating tool and gravity settled. The amount of the solution is a function of the desired thickness of the sensitive layer. For example, if we want to obtain a 80 μm dry layer, we are to take 0.04 cm^3 of the solution on each 1 cm^2 of a glass plate. After the deposition, the layer is dried in dark under normal laboratory conditions (temperature 22 °C and 40 % relative humidity) for about 24 hours. The dry layer of the recording material is not in the solid state but it can be characterized as a tough gel permeable for small molecules such as monomers. As the monomer concentration is relatively high, precipitation of it on the surface of the layer may occur during storage and so the material becomes unusable for the measurements. The precipitation can be avoided, if a thin cover glass is attached on the layer with a cyanoacrylate glue just after drying. Another way is covering the surface with a clear lacquer.

4. Measuring method and experimental setup

The material is tested with the continuous measurement of the diffraction efficiency of a forming grating during holographic exposure. Martin et al. (1997); Moreau et al. (2002); Rhee et al. (1995), and others have been already used methods with the similar principle. Usually, only the time measurements of the diffraction efficiency were obtained that is not sufficient for a material characterization. The diffraction efficiency is a parameter describing the quality of a diffraction grating, but the recording material is better characterized with the refractive index modulation. Refractive index is more closely connected with the chemical composition of a recording material and its changes can be used for describing the processes running within the recording material.

A quantity of the refractive index modulation is determined from the measurement of the diffraction efficiency with Eq. (18) derived in the coupled wave theory (Kogelnik (1969)). The efficiency is measured with a wavelength which is different from the recording one. It is chosen from the non-absorbing band of the recording material and so the measurement does not influence the recording process. As the recording process can be non-linear and higher harmonics can arise, the detection method has been recently extended to the measurement of the diffraction efficiency of the second harmonic grating. Both efficiencies are measured at once and the amplitudes of refractive index gratings are determined.

In Fig. 6, a schema of the setup, which enables recording of the diffraction grating and measurement of its diffraction efficiency, is given. The beam from the recording laser is

Solution I	
Polyvinyl alcohol ($M_w = 89000 - 98000$)	5 g
Water	30 cm^3
Solution II	
Triethanolamine	4.2 cm^3
Water	2.8 cm^3
Erythrosine B ($2{,}5 \times 10^{-3}$ M water sol.)	2.2 cm^3
Acrylamide	1.9 g
N,N′-methylene-bis-acrylamide	0.22 g
Acrylic acid	1.84 cm^3
Solution I	20 cm^3

Table 1. Typical chemical composition of the acrylamide-based recording material

expanded, filtered, and collimated through the spatial filter and collimating lens. The formed plane wave is divided into two parts. One half of it comes through the material directly and the second half is reflected by the mirror. Both then overlap and form the harmonic interference field which is finally recorded. The recording material is placed symmetrically into the interference field which is perpendicular to the surface of the recording material where a volume phase transmission grating is formed.

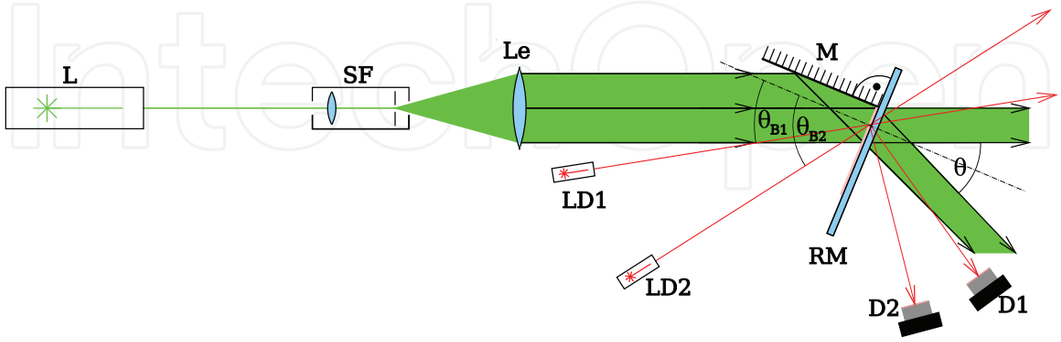

Fig. 6. A schema of the experimental setup. Legend: L - recording laser (532 nm), SF - spatial filter, Le - collimating lens, M - plane mirror, RM - recording material, LD1, LD2 - laser diodes (656 nm), D1, D2, D3 - photo-detectors.

A narrow beam of the detection laser diode (LD1), which wavelength is out of the absorption band, is incident at the Bragg angle θ_{B1} on the recording material. When the beam is passing through the grating, a diffracted beam is generated. The power of the beam is continuously measured with the detector (D1). The second harmonic grating is detected with the laser diode (LD2) which is adjusted at the Bragg angle θ_{B2} of the second harmonic grating. The power of the diffracted beam is detected with the detector (D2). The exposure and the measurements proceed simultaneously.

The interference field is unslanted in the recording medium. The period of the interference field Λ is given by the expression

$$\Lambda = \frac{\lambda}{2\sin\frac{\theta}{2}}, \tag{15}$$

where λ is the wavelength of recording light and θ is the angle between incident waves (in the air). The first harmonic grating has the same spatial period as the interference field and the period of the second harmonic grating is $\Lambda/2$.

The volume phase transmission grating is very selective with respect to the reconstruction angle. The maximum diffraction efficiency is obtained at the Bragg angle. Bragg angles can be evaluated from Eq. (15) where the reconstruction wavelength λ_r, period of the first harmonic grating Λ and period of the second harmonic grating $\Lambda/2$ are substituted;

$$\theta_{B1} = \operatorname{asin}\frac{\lambda_r}{2\Lambda} \qquad \text{and} \qquad \theta_{B2} = \operatorname{asin}\frac{\lambda_r}{\Lambda}. \tag{16}$$

The diffraction efficiency is a ratio of the diffracted power to the incident power. It can be evaluated from the real-time measurement of power $P_{d1}(t)$, power $P_{d2}(t)$, of the diffracted beam, respectively and power P_{i1}, P_{i2} of the incident beam, respectively.

$$\eta_1(t) = \frac{P_{d1}(t)}{P_{i1}} \qquad \text{and} \qquad \eta_2(t) = \frac{P_{d2}(t)}{P_{i2}}. \tag{17}$$

First harmonic grating

The efficiency η_1 and the refractive index modulation n_1 relate through the equation derived in the coupled wave theory.

$$\eta_1 = \sin^2 \frac{\pi n_1 d}{\lambda_r \cos\theta_{B1}}, \tag{18}$$

where d is the thickness of a recording layer, λ_r is the reconstruction wavelength and θ_{B1} is the Bragg angle. The refractive index modulation is evaluated as an inverse function to (18) and hence it is given with the expression

$$n_1 = \frac{\lambda_r \cos\theta_{B1}}{\pi d} \operatorname{asin}\sqrt{\eta_1}, \tag{19}$$

for $n_1 \in \langle 0, \lambda_r/(2d)\cos\theta_{B1})$. The function (18) is not a uniquely invertible function and so when the overmodulation occurs, $n_1 \in \langle \lambda_r/(2d)\cos\theta_{B1}, \lambda_r/d\cos\theta_{B1})$, the refractive index modulation equals

$$n_1 = \frac{\lambda_r \cos\theta_{B1}}{\pi d} \left(1 - \operatorname{asin}\sqrt{\eta_1}\right). \tag{20}$$

Second harmonic grating

The relation between the efficiency η_2 and the second harmonic amplitude n_2 was derived in the extended coupled wave theory (Benlarbi & Solymar (1980a;b)). The analytical solution of the coupled wave equation was revised and used for calculations of the second harmonic grating strength by Zhao & Mouroulis (1995). The equation is given by

$$\eta_2 = \sin^2 \left[\frac{\pi d}{\lambda_r \cos\theta_{B2}} \left(n_2 - \frac{n_1^2}{n_0 \sin^2\theta_{B2}} \right) \right], \tag{21}$$

where θ_{B2} is the Bragg angle of the second harmonic grating and n_0 is the mean value of the refractive index. The second harmonic amplitude of the refractive index modulation is again evaluated as an inverse function to Eq. (21) and hence it is given with the expression

$$n_2 = \frac{\lambda_r \cos\theta_{B2}}{\pi d} \operatorname{asin}\sqrt{\eta_2} + \frac{n_1^2}{n_0 \sin^2\theta_{B2}} \tag{22}$$

for $n_2 \in \langle 0, \lambda_r/(2d)\cos\theta_{B2} + n_1^2/(n_0 \sin^2\theta_{B2})\rangle$. It can be seen, that the value n_1 must be known for determination of the second harmonic amplitude n_2. Usually, the second harmonic grating is not overmodulated, because the value n_2 is relatively small and hence only the unique inversion is assumed.

In the Kogelnik's coupled wave theory, higher diffraction orders are neglected due to violation of the Bragg condition. In reality, very weak higher diffraction orders may arise even in a thick recording medium. We analyzed possible higher diffraction orders of the first harmonic grating and compared them with diffraction orders of the second harmonic grating. It was found that the diffraction angles, which correspond to higher orders of the first harmonic grating, are completely different from the diffraction angles of the second harmonic grating. Therefore the measurement of the diffraction efficiency of the second harmonic grating is not influenced with the measurement of the first harmonic grating. Both measurements are independent and thus they can be carried out simultaneously.

4.1 Experimental setup

The exposure and detection setup is placed on the optical table which is isolated and damped from surrounding vibrations (see Fig. 7). For the exposure, the diode-pumped, frequency-doubled Nd:YAG laser (L), that emits at a 532 nm wavelength, is used (Coherent model 532-400). The beam from the laser passes through the electronically controlled shutter (S). The attenuator (A), which reduces power of the beam, is the next optical component. With the attenuator, the required optical intensity incident on the recording material is adjusted. The beam then passes through the spatial filter (SF) where it is focused and spatially filtered. The divergent wave from the filter is collimated with the lens (Le) to form a quasi plane wave. One half of it is incident directly on the recording material placed in the mount (H) and the other half is reflected with the mirror which is firmly fasten to the mount. Both waves overlap and create a harmonic interference field in the place where the sample is located.

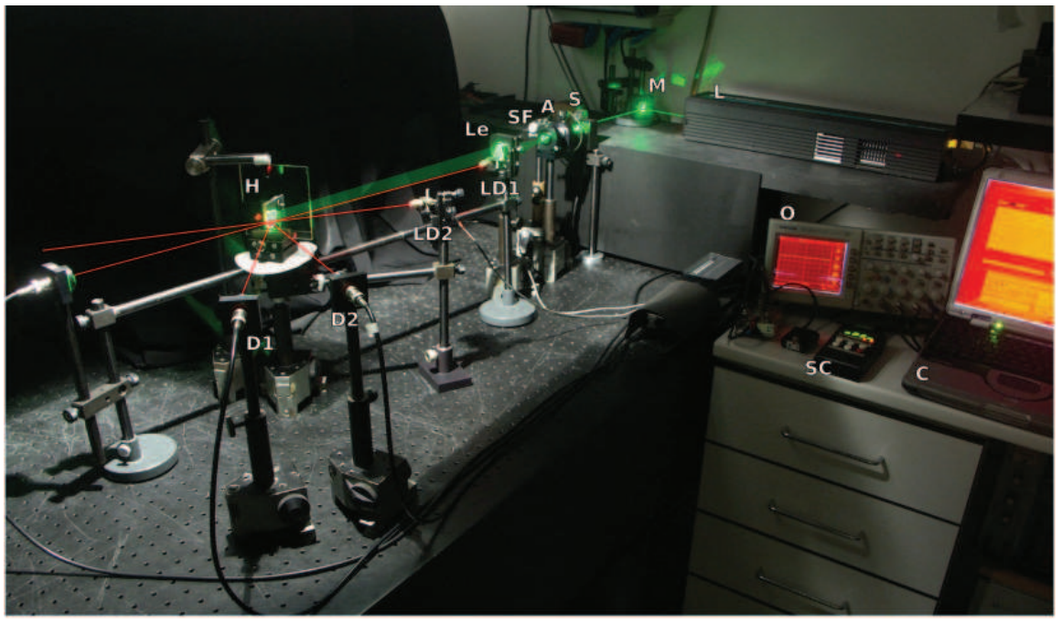

Fig. 7. Experimental setup used for the real-time measurements.

The detection part of the setup is composed of laser diodes (LD1, LD2), optical detectors (D1, D2) and oscilloscope (O). The standard collimated laser diodes at a 656 nm wavelength and 5 mW output power are used. The power of diffracted and passing beams is detected with PIN photodiodes. The measured optical power ranges from 0 to 5 mW. The photodiodes are wired in a reverse bias voltage mode to provide a high linearity. When illuminated, it generates a current passing through a load resistance on which the voltage is measured with the oscilloscope. The digital storage oscilloscope is used for the measurement of signals from photodiodes.

The exposure and measurement is operated with the shutter-control (SC). It operates the shutter which opens and closes the recording beam and also triggers the oscilloscope measurement. The acquired data are stored in the memory of the scope and can be transferred through the serial line to a computer for further processing.

4.2 Measurement and data processing

Before the measurement, exposure parameters such as overall recording intensity, period of the interference field, and exposure time are adjusted. The intensity is accurately set with the attenuator (A).The spatial period of the interference field is adjusted by rotating with mount (H) around its vertical axis. The value of the period is determined from the angle between recording waves with Eq. (15). Finally, the exposure time is set on the shutter-control which operates the exposure and measurement.

Laser diodes must be adjusted at Bragg angles. Firstly, laser diode beams are roughly directed at calculated Bragg angles (Eq. (16)). Secondly, a test sample of the grating is recorded and angles of detection beams are precisely adjusted at maximum diffraction efficiency which is measured with the detector. The measured voltage is linearly proportional to the optical power on the detector; the constant of proportionality has been determined experimentally.

Before the exposure, the sample of the recording material is placed to the mount and fixed with a small clamp against shifting. The size of each sample is typically $2 \times 2\,\mathrm{cm}^2$ and xylen is used as an immersion liquid to prevent reflections on boundaries between the sample and the mount. Other losses caused by Fresnel reflections on boundaries are eliminated during evaluation of the diffraction efficiency. Noise of the recording material and possible higher diffraction orders are negligible.

The shutter-control starts the exposure and measurement. The grating continuously grows up which is measured with detectors in the real-time. The diffraction efficiency is calculated with Eq. (17) from the acquired data. For evaluation of the refractive index modulation (Eq. (19)), the thickness of the sample layer must be known. It is measured with a mechanical profilometer after each exposure. In Fig. 8, an example of measured diffraction efficiency $\eta_1(t)$ and evaluated refractive index modulation $n_1(t)$ of the forming grating are presented. As was already mentioned, the plot of the refractive index modulation on time is the grow-curve.

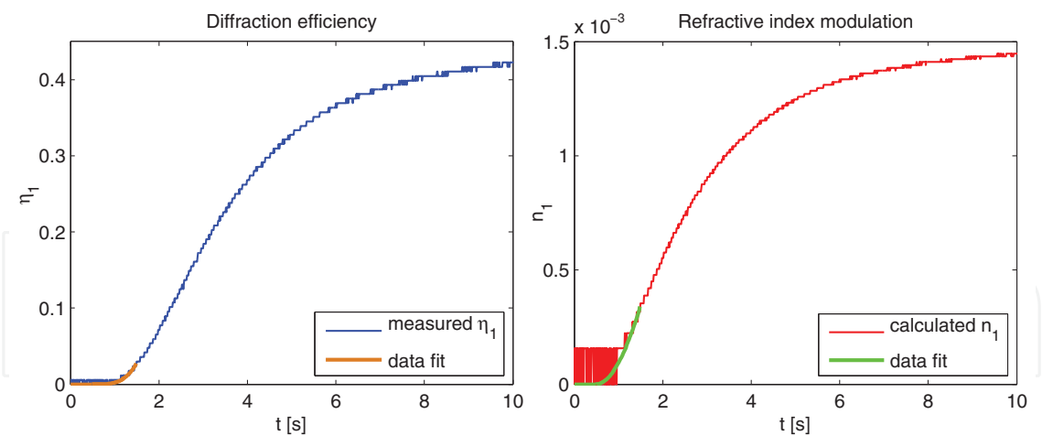

Fig. 8. Time variations of the diffraction efficiency and refractive index modulation. Exposure parameters: $\Lambda = 700\,\mathrm{nm}$ and $I_1 = I_2 = 1.3\,\mathrm{mW/cm}^2$.

The time resolution of the data measured with the oscilloscope is excellent. The typical curve is composed of 2500 points (see Fig. 8). The noise at low values of the diffraction efficiency is due to the reverse bias mode of the photodiode and also due to the low voltage resolution of the digital oscilloscope. This relatively low noise is even more amplified when the refractive index modulation is evaluated. The main cause of this problem is Eq. (19). If we analyze the

differential of Δn_1, it can be seen that it depends non-linearly on the differential of $\Delta\eta_1$:

$$\Delta n_1 = \frac{\mathrm{d}n_1}{\mathrm{d}\eta_1}\Delta\eta_1 = \frac{\lambda\cos\theta_{B1}}{2\pi d}\,\frac{1}{\sqrt{\eta_1 - \eta_1^2}}\Delta\eta_1. \tag{23}$$

A small deviation $\Delta\eta_1$ at low values of efficiencies ($\eta_1 \to 0$) is very much amplified and it results in a large deviation of Δn_1. It complicates the interpretation of beginning parts of the grow-curve; mainly the initiation time of the growth is difficult to find.
The problem with a noise for low signals can be reduced when the measurement is performed twice with the same exposure conditions. At first, the whole measurement is done with the reverse biased photodiode. At second, the photodiode is wired in the unbiased mode and the measurement is performed with a new sample and the same exposure conditions. In this mode, the photodiode has a high sensitivity and a low noise. However, the detection range is limited only to low values of the optical power as the saturation of the photodiode occurs. The initial part of the curve is now measured very precisely and hence the initiation time can be found. Finally, we replace the measured noise data from the reverse biased mode with the data obtained in the unbiased mode before the saturation of the detector and the whole curve of the refractive index modulation is evaluated without the noise. In Fig. 8, the preciously measured data (data fit) are also presented.

5. Experimental results and findings

Conventional recording materials such as silver-halide emulsions or dichromated gelatin are characterized with measurements of the diffraction efficiency which are obtained after processing. In the optimization procedure, several test gratings must be recorded, processed, and measured to find optimal values of exposure parameters. In photopolymers, the real-time detection method enables to obtain more characteristics at once (the grow-curve). However, the behavior of a photopolymer material is more complicated. The reciprocity law (a relation connecting the optimal value of the exposure energy with exposure time and recording intensity) is not valid and also the performance of the material strongly depends on other parameters such as the spatial period of the interference field or chemical composition of the recording system.
Within our work on this topic, a large number of measurements have been carried out. The detection method and experimental setup have been continuously improved and also the accuracy of the measurements. The selected results, which are here presented, describe our main findings. Some more experimental results have been already published in our recent papers (Květoň et al. (2007; 2008)).

5.1 The grow-curve

The grow-curve describes the process of the diffraction grating formation through the parameter n_1. The typical grow-curve is illustrated in Fig. 9 where the formation process is divided into four recording phases:

I – induction period. At the beginning of exposure, a short induction period of the length t_i is observed; no refractive index modulation is detected. In spite of no detectable change of the refractive index, some initiation processes may be running in the recording material.

II – exposure growth. At time t_i, the growth of the grating begins. This phase is interrupted at exposure time t_e when the recording laser is switched off. The rate of a grating formation

depends on exposure parameters and a chemical composition of the material. Typically, the formation rate increases in the beginning of this phase. The grow-curve goes through its inflexion point and the formation rate decreases at the end of the exposure phase.

III – post-exposure growth. An additional increase of the refractive index modulation occurs. The growth is not interrupted immediately at t_e even if the exposure is switched off. It runs out successively and saturates as the formation rate decreases to zero. This phase also strongly depends on exposure parameters and a material composition.

IV – final period. In the final period, the refractive index modulation remains stable or it may slowly decrease in time. The decrease is caused by degradation processes and its rate depends on the value of n_1 and chemical composition of the material. In fact, the degradation process may already be running from the beginning of the grating growth, but it is observed only at later exposure times when the grow rate decreases.

The phases of the grow-curve have been analyzed further in a more detail. They depend on both the exposure conditions and chemical composition.

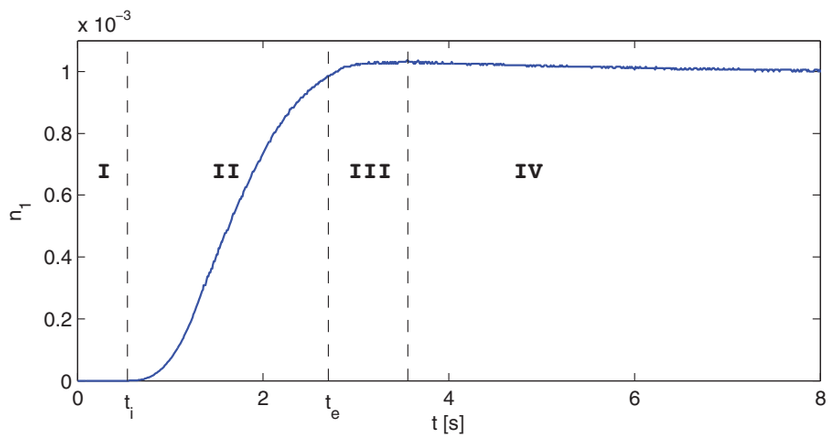

Fig. 9. Phases of the grow-curve. I – induction period, II – exposure growth, III – post-exposure growth, IV – final period.

Volume phase transmission gratings with the diffraction efficiency close to 1 are produced in the recording material given in Tab. 1. This efficiency corresponds to the value of n_1 of the order 10^{-3} ($n_{1max} = 4 \times 10^{-3}$). However, the maximum value is strongly dependent on exposure conditions and chemical composition, already mentioned above. Also the laboratory conditions, which occur during the preparation procedure and measurements (e.g. humidity, temperature), influence the performance of the material (grow rate, n_{1max}). So if we compare measurements at different exposure conditions, they have been performed on samples of the recording material prepared at the same laboratory conditions to avoid misinterpretations.
The optimal exposure energy is a parameter of a special interest in recording materials. It is defined as the amount of radiation received by a surface per unit area and it is calculated as a product of the incident intensity and time. Waves can be incident at angles different from the normal to the surface and so cosine factors must be considered. The interference field is formed by two waves of intensities I_1 and I_2 which are incident at angles θ_1 and θ_2 and so the exposure energy is

$$E = (I_1 \cos\theta_1 + I_2 \cos\theta_2)\, t. \tag{24}$$

In conventional recording materials, the reciprocity law is often assumed

$$E_{opt} = It_e, \tag{25}$$

where intensities and cosine factors are included in the overall recording intensity termed I. The reciprocity law says that the product of the overall recording intensity I and the exposure time t_e has the same efficiency independently on the ratio of I to t_e. There are some small deviations from the reciprocity law for very low and high intensities even in conventional materials. The deviations from the reciprocity are more prominent in the case of photopolymers. At lower recording intensities, E_{opt} is usually lower.

5.2 Influence of exposure parameters

5.2.1 Induction period

The length of the induction period t_i depends mainly on the recording intensity. In the case of a higher recording intensity, the induction period is shorter than that in the case of a lower intensity, as can be seen in Fig. 10 (a).

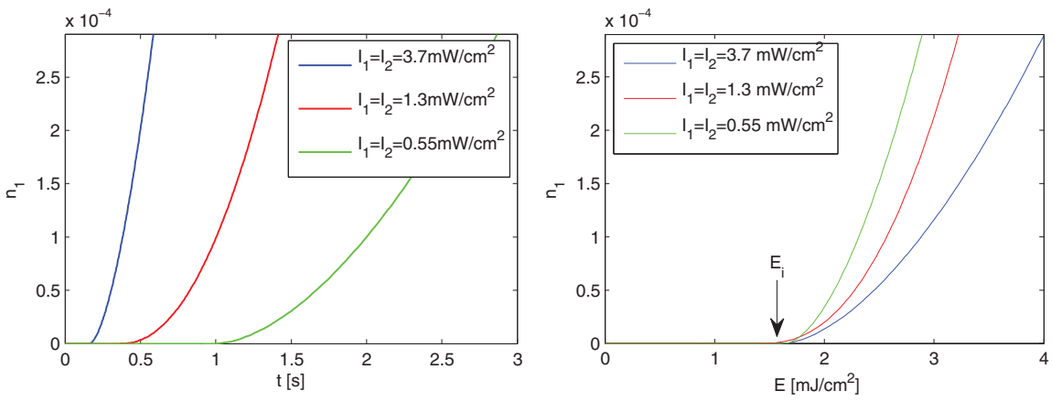

(a) grow-curves – induction periods (b) E-n_1 curves – initiation energies

Fig. 10. Measurements of induction periods and the calculated E-n_1 curves for different recording intensities (Λ=0.7 μm).

Measurements for different values of the intensity and the spatial period of the recording interference field were done and the results of induction times t_i are given in Tab. 2. For the same exposure intensities, the value of t_i is very similar for all periods of the interference field. Relatively small differences are due to the short spatial period cut-off. In the case of $\Lambda_1 = 0.45\,\mu$m, a grating with a very low value of the refractive index modulation is formed, in comparison with $\Lambda_3 = 2\,\mu$m. Therefore, it is assumed that the first detectable changes are slightly shifted in time.

In Fig. 10 (b), exposure energy variations of n_1 are given for the same measurements. A linear relation between the exposure energy and time is given by Eq. (24) where the constant of proportionality is the overall intensity. It can be seen that the dose of the induction exposure energy E_i is very similar for all recording intensities. The values of E_i were evaluated also for other spatial periods and recording intensities and the results are summarized in Tab. 2 (the values in brackets).

At the beginning of polymerization, the effect of inhibition with polymerization suppressors is described (Odian (2004)). We assume that the induction period is caused by oxygen as

Intensity $I_1 = I_2$	t_i [s] (E_i [mJ/cm^2])					
[mW/cm^2]	$\Lambda_1 = 0.45\,\mu$m		$\Lambda_2 = 0.7\,\mu$m		$\Lambda_3 = 2\,\mu$m	
0.55	1.70	(1.51)	1.70	(1.73)	1.40	(1.53)
1.3	0.70	(1.47)	0.63	(1.51)	0.55	(1.42)
3.7	0.30	(1.79)	0.25	(1.71)	0.22	(1.60)

Table 2. Measured induction times t_i and calculated initiation energies E_i (given in brackets) for different exposure intensities and spatial periods of the recording interference field.

it is present in the recording layer due to the preparation procedure. It reacts preferably with primary radicals and thus inhibits the standard polymerization reaction of monomers. The dose of E_i is the energy which must be delivered to the photopolymer system to consume all molecules of oxygen. Each sample of the recording material contains a similar amount of oxygen and therefore the same dose of E_i applies. After this induction period, the polymerization of monomers normally proceeds and the change of the refractive index is detected. The theoretical models do not include the effect of inhibition and so the grow-curves start to rise from the very beginning.

5.2.2 Exposure growth

After the induction period, the grating starts to grow. At the beginning of this phase, the rate of growth rises up. When the grow-curve reaches its inflexion point, the rate of growth starts to decrease and a saturation of the grow-curve occurs (even if the exposure continues). In the case of a higher recording intensity, a higher recording rate is detected than that in the case of a lower recording intensity (see Fig. 11 (a)). The effect of intensity can by theoretically explained by the both diffusion models. The polymerization rate depends on the recording intensity. If a higher recording intensity is applied, the polymerization proceeds at the higher polymerization rate and so the grating growth is faster than that in the case of a lower recording intensity.

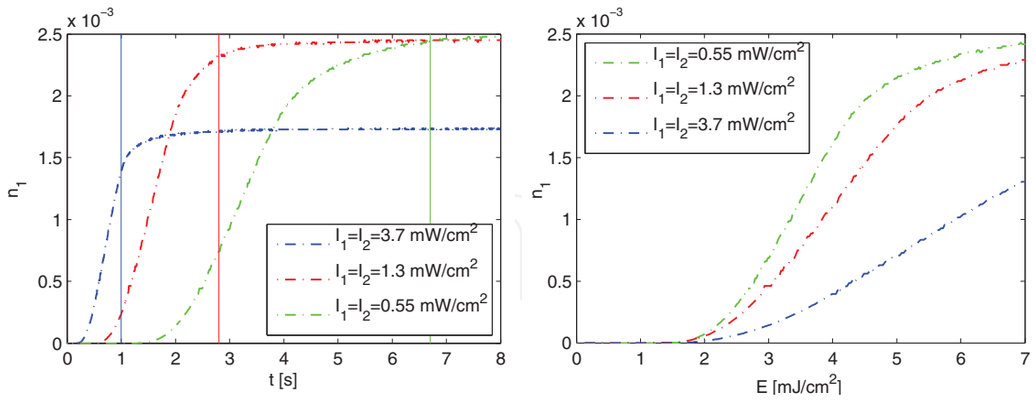

(a) grow-curves (b) E-n_1 curves

Fig. 11. Comparison of measured grow-curves and calculated E-n_1 curves for different recording intensities (Λ=2 μm).

In Fig. 11 (a), the exposures are interrupted at 1, 2.8, and 6.7 s (the times of interruption t_e are marked with appropriate vertical lines). At these times, the exposure energies are similar in all three case, but the values of n_1 differ. To show the reciprocity law Eq. (25) failure, we have

plotted the measured refractive index modulation n_1 versus exposure energy E. It follows, that a lower recording intensity requires less energy to achieve the same value of n_1. So the exposure process is more effective for low recording intensities. It seems better to use longer exposure times at lower intensities to obtain a higher index modulation and hence a more efficient grating. However, the exposure time is a crucial parameter. A fine interference field is not stable enough for long lasting exposures and also some other degradation effects, which will be discussed further, may negatively influence the formation process.
The grating growth depends strongly on the spatial period of the interference field. The grow-curves of different spatial periods and the same recording intensities are compared in Fig. 12. In the case of a long period ($\Lambda = 2\,\mu$m), the grating grows up rapidly and a high value of the refractive index n_1 is reached. On the other hand, a short spatial period ($\Lambda = 0.45\,\mu$m) is difficult to record. It is caused by a limited resolution of the acrylamide based material that ranges from 0.5 to 5 μm. For spatial periods longer than 2 μm, a relief grating is also formed, higher diffraction orders are produced and the detection method becomes inconvenient.

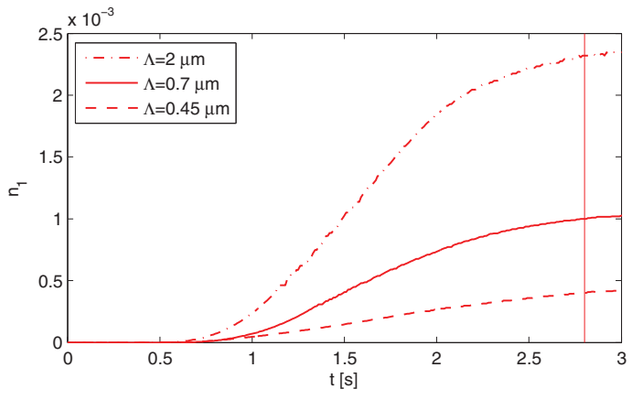

Fig. 12. The grow-curves for different spatial periods of the recording interference field ($I_1 = I_2 = 1.3\,\mathrm{mW/cm^2}$, $t_e = 2.8\,$s).

5.2.3 Post-exposure growth

The grating growth continues even if the exposure is interrupted. The post-exposure growth is a part of the grow-curve between the point of interruption t_e and the maximum of the grow-curve. In Fig. 13, the exposures of similar samples have been interrupted at different exposure times (2, 4, and 7 s). The highest value of the post-exposure increase ($\Delta n_1 = 1.4 \times 10^{-4}$) was obtained when the exposure was interrupted at t_e=2 s (red curve).
The magnitude of the post-exposure growth depends on the grow rate of the grating at the interruption time. In the case of a higher grow rate (usually at early stages), the post-exposure growth is larger than that in the case of lower grow rates. To verify this observation, the post-exposure growth was measured for different spatial periods and intensities of the interference field (see Fig. 14). At first, the samples were exposed with the same exposure intensities ($I_1 = I_2 = 3.7\,\mathrm{mW/cm^2}$, $t_e = 1\,$s) but three different spatial periods of the interference field were used. In Fig. 14 (a), it can be seen that the additional increase decreases with shortening of the spatial period. At second, the post-exposure increase for different recording intensities was measured (see Fig. 14 (b)). The spatial period was set to 2 μm and the dose of exposure energy was similar in all three tested samples. The largest additional

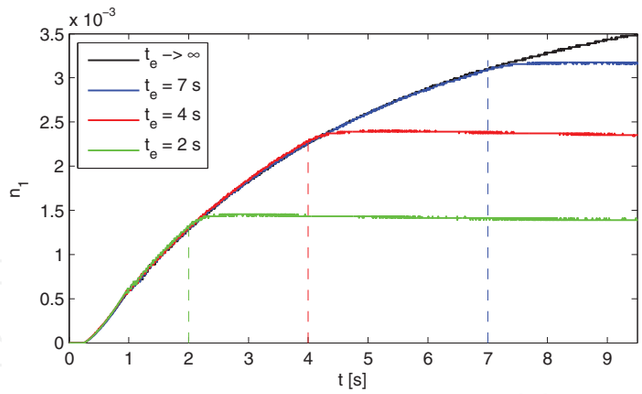

Fig. 13. Post-exposure growth – the exposure was interrupted at $t_e = 2,\ 4,$ and $7\,s$ ($\Lambda = 0.7\,\mu$m and $I_1 = I_2 = 3.7\,\mathrm{mW/cm^2}$).

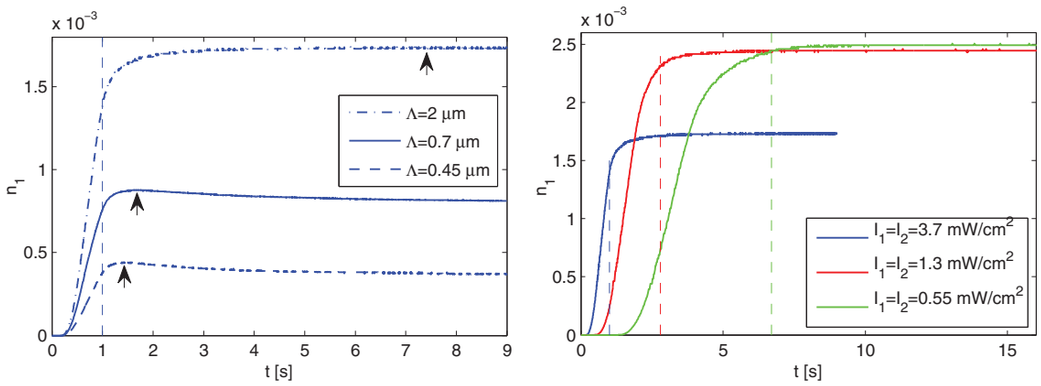

(a) (b)

Fig. 14. Post-exposure growth – influence of spatial periods (a) and recording intensities (b).

increase is observed for the highest recording intensity. A similar behavior was found also for other tested spatial periods.

The effect of the post-exposure growth is usually explained with the diffusion model. At the interruption time t_e, a gradient of monomer concentration is formed in the recording material. After the exposure, radicals recombine very rapidly and so the post-exposure growth is ascribed only to the diffusion of monomers from dark to bright places. This diffusion process continues until the gradient vanishes.

From our complementary measurements (electron paramagnetic resonance) follows that the life-time of radicals is relatively long. Hence the polymerization process continues even after the exposure until the radicals recombine. It seems more probable that the post-exposure growth is caused by remaining radicals. Our conclusion is also supported with the recent measurements of the diffusion process in acrylamide photopolymers performed by Babeva et al. (2008). It has been found that the diffusion coefficient is much higher than that assumed in previous studies. The diffusion of monomers is very fast and so the magnitude of the concentration gradient is irrelevant. These results are in agreement with the ID-theory where no concentration gradient is supposed.

5.2.4 Final period

The refractive index modulation remains stable or slowly decreases after the exposure. Sometimes, a decrease of n_1 is observed already during long lasting exposures. A decrease of the refractive index modulation is assigned to the degradation process. The degradation process starts already at the beginning of the formation process but the formation process is much more dominant and therefore, a decrease of n_1 is not observed. The degradation process shows out at later times when the value of n_1 is high and the formation rate starts to decrease. In contradiction to the exposure and post-exposure growth, the degradation does not depend much on the recording intensity. A comparison of the degradation processes of gratings recorded with different intensities is given in Fig. 15.

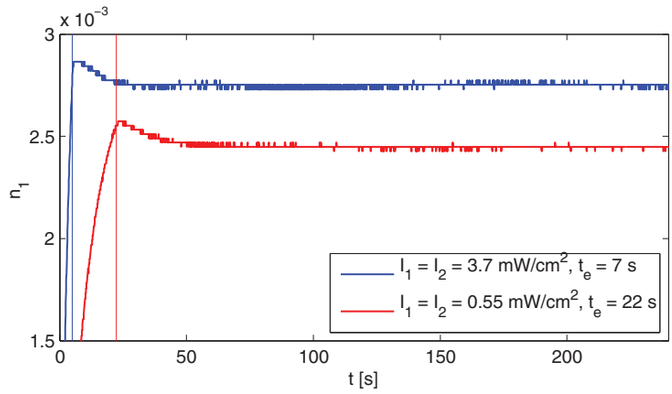

Fig. 15. Degradation process of the diffraction grating ($\Lambda = 0.7\,\mu$m).

The degradation rate depends on the spatial period of a grating formed, as may be also seen in Fig. 14 (a). The relative decrease of n_1 is 17% for $\Lambda = 0.45\mu$m, 7% for $\Lambda = 0.7\mu$m, and 1% for $\Lambda = 2\mu$m, 9 s after the interruption of the exposure. The gratings with larger spatial periods are more stable and also their values of the refractive index modulation are higher.

The degradation process is not included in the diffusion model describing formation of the grating in photopolymers; it is assumed that a grating formed is stable due to immobility of polymers. This is not true because the opposite diffusion of polymers occurs due to their concentration gradient. The mobility of polymers is much lower than that of monomers but it should not be automatically neglected. This is taken into account in the ID-theory. In the next section, it will be shown that the polymer mobility can be decreased by addition of a crosslinker and so the stability of the grating is increased.

In the case of DuPont or Polygrama photopolymers, additional processes are involved to fix or even improve characteristics of diffraction gratings formed. The grating is stabilized by the post-exposure with a homogeneous illumination. In the case of acrylamide-based photopolymers, the post-exposure illumination speeds up the degradation effect. Experiments of post-exposure illumination were carried out. The value of the refractive index modulation dropped to its half value after the exposure but the final grating was stable and no additional decrease of n_1 was observed. This effect is not very clear and more experiments have to be done to clarify it.

5.3 Influence of the chemical composition

Monomers and crosslinker are fundamental for the process of the grating formation. Acrylamide (AA), acrylic acid (AAC), and methylene-bis-acrylamide (BAA) influence the

recording process in different ways. Each molecule differs in polymerization rate, size, structure, or diffusion ability. A high value of the refractive index change is desired and so a high concentration of monomers in the recording layer is necessary. Unfortunately, the crosslinker BAA is very badly soluble in water and hence layers with a high concentration can not be prepared. A very high concentration of AA produces opaque layers due to its precipitation. Finally, gratings formed in layers composed of only AAC are not stable enough and degrade rapidly in time.

Samples of the recording material with a different composition of monomers were prepared and tested to show the influence of different monomers on the recording process. In each sample of the recording layer, the concentration of C=C double bonds of all monomers was similar. Molecules of AA and AAC include only one double bond, BAA has two double bonds which both may radically polymerize. The concentrations of remaining components were exactly the same in each sample (see optimized material composition in Tab. 1). Contents of monomers in the recording layer are summarized in Tab. 3 and the results of the measurements are given in Fig. 16.

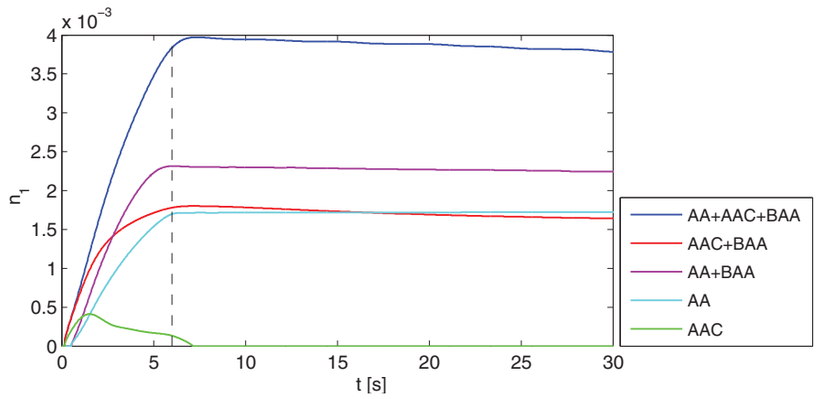

Fig. 16. Grow-curves of materials with different contents of monomers ($I_1 = I_2 = 3.7\,\mathrm{mW/cm^2}$, $\Lambda = 0.7\,\mu\mathrm{m}$, and $t_e = 6\,\mathrm{s}$).

If only AA (cyan line) is present in the layer, the grating forms slowly and a low value of the refractive index modulation n_1 is reached. The formed grating is stable and even a slow increase of n_1 is observed in the phase IV. Addition of crosslinker (AA+BAA – magenta line) increases the rate of grating growth. A higher value of n_1 is obtained but the refractive index modulation slightly decreases after the exposure proceeds.

If only AAC (green line) is added, the grating starts to form early but the rate of grating formation is low. The maximum value of n_1 is low and a decrease of n_1 can be observed already during the exposure. When the exposure is interrupted, the modulation decreases very quickly to zero and the grating is completely erased. If a small amount of crosslinker is added (AAC+BAA – red line), the rate of the grating formation increases. The length of the induction period is shorter than that in the case of the material with AA+BAA (magenta line). The rate of formation changes from high on the beginning to low at the end of the exposure process. After exposure, a small decrease of n_1 is measured.

The grating, which is formed in the recording material with both monomers and crosslinker (AA+AAC+BAA - blue line), starts to grow very early. Its grow rate is high and large value of n_1 is reached at time t_e. The post-exposure growth can be observed but also the degradation process. The results of all materials are summarized in Tab. 3.

Monomer	Ratio AA:AAC:BAA	t_i [s]	$n_1(6\,\mathrm{s}) \times 10^{-3}$	$n_1(30\,\mathrm{s})/n_1(6\,\mathrm{s})$
AA	100:0:0	0.27	1.72	1.02
AA+BAA	95:0:5	0.25	2.33	0.97
AAC	0:100:0	0.23	0.13	0
AAC+BAA	0:95:5	0.2	1.82	0.92
AA+AAC+BAA	47.5:47.5:5	0.17	3.85	0.99

Table 3. Characteristics of recording materials with different compositions of monomers.

It was demonstrated that addition of the crosslinker increased the grow rate. This effect has been predicted with the ID-theory. The crosslinker concentration is characterized with the immobilization exponent m; the exponent increases with an increasing amount of the crosslinker. Branching and networking of polymers occur even when a small amount of the crosslinker is added. Stabilization of the branched polymer is faster and its opposite diffusion is much more difficult.

5.4 Detection of the second harmonic grating

The recording process is non-linear and so higher harmonics are formed even if the recording material is exposed with the harmonic interference field. Next to the first harmonic grating with the same elementary period as the interference field, a second harmonic grating is formed with the half period. The detection method of the second harmonic grating has been introduced in section 4. The first and second harmonic amplitude of the refractive index are plotted together in one figure for a comparison (see Fig. 17). Typically, the first harmonic grating starts to grow first. The second harmonic appears later when the first reaches a specific value. Both amplitudes then continue in growth. The maximum of the first amplitude is reached at a different time (usually much earlier) than that of the second harmonic grating. When the exposure goes on, the first harmonic amplitude n_1 may start to decrease due to the degradation process but the growth of the second harmonic continues.

5.4.1 Influence of the spatial period

First and second harmonic amplitudes were measured for different spatial periods of the recording interference field (see Fig. 17). In the case of a short period ($\Lambda = 0.7\,\mu$m), n_1 is lower than that for longer periods and values of n_2 are almost undetectable. Such a grating has nearly ideal harmonic profile. In the case of longer spatial periods ($\Lambda = 2\,\mu$m), higher values of n_1 are obtained but also a relatively high n_2 is formed. The recording process is more non-linear.

A lower value of n_2 relates to lower resolution of the material at short spatial periods. The period of the second harmonic frequency is two times shorter than that of the first harmonic. So in the case of spatial period $0.7\,\mu$m, the second harmonic period is only $0.35\,\mu$m which is out of the resolution of the medium and hence the second harmonic grating is not formed.

5.4.2 Influence of the recording intensity

A significant non-harmonic profile is produced when the recording interference field with a large spatial period is applied. The period of the interference field was set to $2\,\mu$m and measurements with different exposure intensities were carried out. The results are presented in Fig. 18. Dependences of n_1 and n_2 on the exposure energy E are given for a better comparison of all displayed curves.

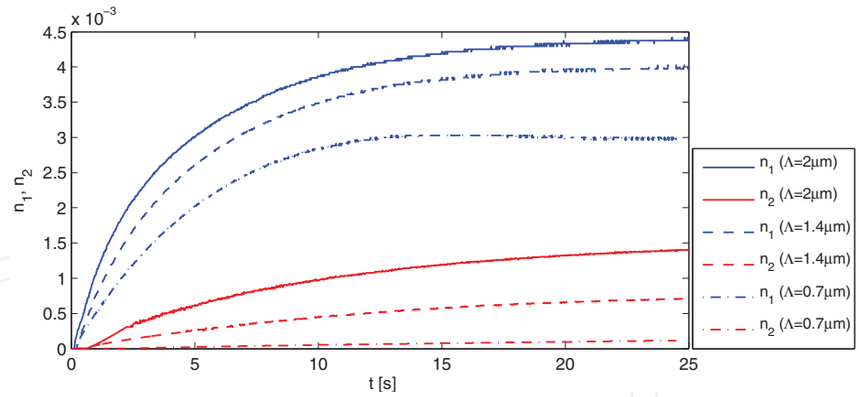

Fig. 17. Grow-curves of n_1 and n_2 obtained with the exposure of different spatial periods ($I_1 = I_2 = 3.7\,\mathrm{mW/cm^2}$).

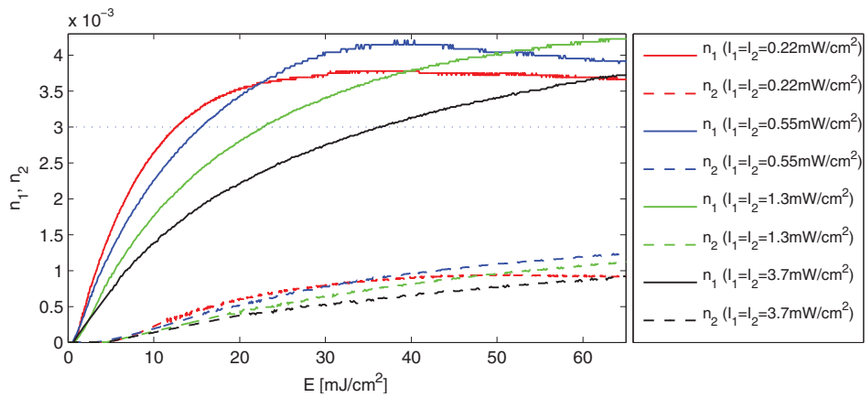

Fig. 18. Dependences of the first and second harmonic amplitudes on the exposure energy for different intensities of the recording interference field (spatial period was 2 μm). The reference value of n_1 is marked with the dotted line.

The saturation values of n_1 and n_2, respectively are very similar for all recording intensities. Usually, the exposure is interrupted when n_1 reaches a sufficiently high value. So we chose a number $n_1 = 3 \times 10^{-3}$ as the reference value for the examination of non-linearities at different intensities. The quantum of the exposure energy, when the grow-curve reaches the value 3×10^{-3}, is labelled $E_{n_1=3\times10^{-3}}$. The energy varies for different intensities. At this quantum, n_2 is evaluated and is given for a comparison in Tab. 4. In the case of lower recording intensities, n_1 reaches the number 3×10^{-3} at lower exposure energies and a lower amplitude of the second harmonic grating is formed.
It was also found that the post-exposure growth of the second harmonic amplitude is low. The degradation process occurs similarly as in the case of the first harmonic amplitude, but the value of n_2 is lower than that of n_1 and hence a thorough analysis of the post-exposure effects of n_2 is less significant. In general, the non-linear recording process causes undesirable effects. The formation of the second harmonic grating reduces the concentration of monomers available for the growth of the first harmonic grating. Also higher diffraction orders may arise due to non-linearities (thin gratings). The growth of n_2 proceeds at later exposure times and so it can be partially eliminated if the exposure is interrupted earlier.

$I_1 = I_2$ [mW/cm^2]	$E_{n_1=3\times10^{-3}}$ [mJ/cm^2]	$n_2(E_{n_1=3\times10^{-3}})$ $\times10^{-4}$	$n_2 : n_1$
0.22	12.7	3.2	0.11
0.55	15.6	3.8	0.12
1.3	22.7	4.9	0.16
3.7	36.4	6.1	0.2
9.2	77.6	7.1	0.24
36	807	9.9	0.33

Table 4. Comparison of non-linearities for different exposure intensities. Second harmonic amplitudes were evaluated at exposure energies when $n_1 = 3 \times 10^{-3}$.

6. Conclusion

The paper was devoted to the study of acrylamide-based recording material for optical holography. During the holographic exposure, the refractive index of the material changes and a volume phase grating is formed without an additional developing process. The formation process of a grating was described theoretically with the ID-theory. It was shown that the grow-curve obtained from both modelling and measurements could be used for characterization of the self-developing photopolymer recording materials. We measured samples of our laboratory prepared photopolymer with the real-time detection method at different exposure conditions and chemical compositions. Obtained grow-curves were compared and confronted also with the theoretical results. The measurements were performed on the acrylamide-based photopolymer, but the results are valid for other types of photopolymer recording materials. In our laboratory, the photopolymers produced by Polygrama were also tested with our experimental setup and the results were published by Lédl & Květoň (2008). Recently, we have used our results and experience for modification of the acrylamide-based material and prepared samples of the optimized photopolymer which has been successfully used as a recording medium for holographic interferometry and holographic memories (Květoň et al. (2010)).

7. References

Babeva, T., Naydenova, I., Martin, S. & Toal, V. (2008). Method for characterization of diffusion properties of photopolymerisable systems, *Optics Express* 16: 8487–8497.

Benlarbi, B. & Solymar, L. (1980a). An analysis of volume phase gratings at higher Bragg angle incidence, *Int. J. Electronics* 48: 361–368.

Benlarbi, B. & Solymar, L. (1980b). Higher-order modes in non-sinusoidal voluma phase holograms, *Int. J. Electronics* 48: 351–359.

Bjelkhagen, H. I. (ed.) (1996). *Selected Papers on Holographic Recording Materials*, Vol. MS 130, first edn, SPIE, Bellingham USA.

Calixto, S. (1987). Dry polymer for holographic recording, *Applied Optics* 26: 3904–3910.

Close, D. H., Jacobson, A. D., Margerum, J. D., Brault, R. G. & McClung, F. J. (1969). Hologram recording on photopolymer materials, *Applied Physics Letters* 14: 159–160.

Colvin, V. L., Larson, R. G., Harris, A. L. & Schilling, M. L. (1997). Quantitative model of volume hologram formation in photopolymers, *J. Applied Physics* 81: 5913–5923.

Gleeson, M. R. & Sheridan, J. T. (2009). A review of the modelling of free-radical photopolymerization in the formation of holographic gratings, *J. Optics A* 11: 24008–24019.

Hariharan, P. (1996). *Optical Holography: Principle, techniques, and applications*, second edn, Cambridge University Press, Cambridge UK.

Havránek, A. & Květoň, M. (2008). Polymer holography - new theory of image growth, *Macromolecular Symposia* 268: 43–47.

Havránek, A., Květoň, M. & Havránková, J. (2007). Polymer holography II - the theory of hologram growth: Polymer growth detected by holographic method, *Polymer Bulletin* 58: 261–269.

Kogelnik, H. (1969). Coupled wave theory for thick hologram gratings, *The Bell System Tech. J.* 48: 2909–2947.

Květoň, M., Havránek, A., Fiala, P. & Richter, I. (2007). Polymer holography I – method and experiment: Polymerization and networking as a method of permanent holographic record formation, *Polymer Bulletin* 58: 253–259.

Květoň, M., Havránek, A., Fiala, P. & Richter, I. (2008). The experimental study of acrylamide based photopolymer recording materials for applications in optical holography, *Macromolecular Symposia* 268: 115–119.

Květoň, M., Lédl, V., Havránek, A. & Fiala, P. (2010). Photopolymer for optical holography and holographic interferometry, *Macromolecular Symposia* 295: 107–113.

Kwon, J. H., Hwang, H. C. & Woo, K. C. (1999). Analysis of temporal behavior of beams diffracted by volume gratings formed in photopolymers, *J. Optical Society of America B* 16: 1651–1657.

Lédl, V. & Květoň, M. (2008). Characterization and application of new photopolymer recording media for usage in holography, *in* P. Tománek, D. Senderáková & M. Hrabovský (eds), *Photonics, Devices, and Systems IV*, number 71381E in *Proc. SPIE Vol.7138*, SPIE, Prague CZ.

Martin, S., Feely, C. A. & Toal, V. (1997). Holographic recording characteristics of an acrylamide-based photopolymer, *Applied Optics* 36: 5757–5768.

Martin, S., Leclere, P., Renotte, Y., Toal, V. & Lion, Y. (1994). Characterization of an acrylamide-based dry photopolymer holographic recording material, *Optical Engineering* 33: 3942–3946.

Moreau, V., Renotte, Y. & Lion, Y. (2002). Characterization of DuPont photopolymer: determination of kinetic parameters in a diffusion model, *Applied Optics* 41: 3427–3435.

Naydenova, I., Jallapuram, R., Howard, R., Martin, S. & Toal, V. (2004). Investigation of the diffusion processes in a self-processing acrylamide-based photopolymer system, *Applied Optics* 43: 2900–2905.

Neipp, C., Gallego, S., Ortuno, M., Marquez, A., Belendez, A. & Pascual, I. (2003). Characterization of a pva/acrylamide photopolymer. Influence of a cross-linking monomer in the final characteristics of the hologram, *Optics Communications* 224: 27–34.

Odian, G. (2004). *Principles of Polymerization*, fourth edn, Wiley, New Jersey USA.

Reif, F. (1965). *Statistical Physics in Berkeley Physics Course – volume 5*, first edn, McGraw Hill, New York USA.

Rhee, U., Caulfield, H. J., Vikram, C. S. & Shamir, J. (1995). Dynamics of hologram recording in DuPont photopolymer, *Applied Optics* 34: 846–853.

Sheridan, J. T. & Lawrence, J. R. (2000). Nonlocal-response diffusion model of holographic recording in photopolymer, *J. Optical Society of America A* 17: 1108–1114.

Xia, C., Zhu, J., Wang, K., Wang, B. & Liu, L. (2002). Optimization of high-quality photopolymer for holographic recording, *in* D. Hsu, J. Chen & Y. Sheng (eds), *Holography, Diffractive Optics, and Applications*, SPIE, Shanghai China, pp. 239–242.

Zhao, G. & Mouroulis, P. (1994). Diffusion model of hologram formation in dry photopolymer materials, *J. Modern Optics* 41: 1919–1930.

Zhao, G. & Mouroulis, P. (1995). Second order grating formation in dry holographic photopolymers, *Optics Communications* 115: 528–532.

Holography, Research and Technologies

Edited by Prof. Joseph Rosen

ISBN 978-953-307-227-2
Hard cover, 454 pages
Publisher InTech
Published online 28, February, 2011
Published in print edition February, 2011

Holography has recently become a field of much interest because of the many new applications implemented by various holographic techniques. This book is a collection of 22 excellent chapters written by various experts, and it covers various aspects of holography. The chapters of the book are organized in six sections, starting with theory, continuing with materials, techniques, applications as well as digital algorithms, and finally ending with non-optical holograms. The book contains recent outputs from researches belonging to different research groups worldwide, providing a rich diversity of approaches to the topic of holography.

How to reference

In order to correctly reference this scholarly work, feel free to copy and paste the following:

Milan Květoň, Pavel Fiala and Antonîn Havránek (2011). Polymer Holography in Acrylamide-Based Recording Material, Holography, Research and Technologies, Prof. Joseph Rosen (Ed.), ISBN: 978-953-307-227-2, InTech, Available from: http://www.intechopen.com/books/holography-research-and-technologies/polymer-holography-in-acrylamide-based-recording-material

INTECH
open science | open minds

InTech Europe
University Campus STeP Ri
Slavka Krautzeka 83/A
51000 Rijeka, Croatia
Phone: +385 (51) 770 447
Fax: +385 (51) 686 166
www.intechopen.com

InTech China
Unit 405, Office Block, Hotel Equatorial Shanghai
No.65, Yan An Road (West), Shanghai, 200040, China
中国上海市延安西路65号上海国际贵都大饭店办公楼405单元
Phone: +86-21-62489820
Fax: +86-21-62489821

IntechOpen